A Flat-lying Transitional Free Gas to Gas Hydrate System in a Sand Layer in the Qiongdongnan Basin of the South China Sea

Zenggui Kuang[123], Ann Cook[4], Jinfeng Ren[13], Wei Deng[13], Yuncheng Cao[5], and Huimin Cai[6]

[1]National Engineering Research Center of Gas Hydrate Exploration and Development, Guangzhou Marine Geological Survey, Guangzhou 511458, China

[2]State Key Laboratory of Marine Geology, Tongji University, 1239 Siping Road, Shanghai 200092, China

[3]Key Laboratory of Marine Mineral Resources, Ministry of Natural Resources, Guangzhou 510075, China

[4]School of Earth Sciences, The Ohio State University, Columbus, Ohio 43210, USA

[5]College of Marine Sciences, Shanghai Ocean University, Shanghai 201306, China

[6]Schlumberger, Shenzhen 518054, China

Corresponding author: Zenggui Kuang (kzg21001@163.com)

Key Points:

- We discover a gas hydrate system where gas transitions to hydrate in a flat-lying sand layer in the northern South China Sea
- Capillary sealing occurs at the sand-clay interface, preventing upward fluid advection and causes fluids to migrate laterally
- Advecting warm fluids and gas are the primary control on the hydrate and free gas system in this sand layer

Abstract

Most marine gas hydrate systems follow a vertical pattern with hydrate overlying free gas. Here we document the discovery of a gas to hydrate system in a horizontal sand layer in the Qiongdongnan Basin of the South China Sea. Eight wells were drilled by the Guangzhou Marine Geological Survey in 2021-2022 to investigate the occurrence and mechanisms responsible for the formation of the system. We describe a free gas-bearing sand reservoir at the center of the system sustained by advecting hot fluids and gas; away from the advecting zone, the cooler, surrounding sand reservoir is filled with hydrate. Observations at this site show that advective heat has a large control on hydrate formation in sands and may be a key mechanism which allows gas migration within the hydrate stability zone and the formation of high-saturation hydrate in sand layers.

Plain Language Summary

Natural gas hydrate, an ice-like substance composed of water and gas, is commonly found in sediments under the ocean. Most marine hydrate systems follow a vertical pattern where hydrate-bearing sediments overlie free gas-bearing sediments; in addition, most hydrate is hosted in marine muds at low concentration. Here we document a horizontal system that transitions from high concentrations of free gas to high concentrations of hydrate in a horizontal sand layer in the northern South China Sea. Two recent drilling expeditions are conducted to explore this unique system. Seismic and logging data suggests that multiple processes including focused fluid flow, capillary sealing and heat transfer control the formation of the system.

1 Introduction

Natural gas hydrate is an ice-like substance composed of gas molecules encased in water cages (Sloan & Koh, 2007) that is most commonly found in sediments on continental slopes (Kvenvolden & Lorenson, 2001; You et al., 2019). On marine seismic data, the thermodynamic boundary between hydrate and free gas is marked by a bottom simulating reflection (BSR) which is usually a reflection roughly parallel to the seafloor with opposite seafloor polarity (Haacke et al., 2007; Shedd et al., 2012). A vertical distribution where hydrate is above the BSR and free gas is below the BSR is quite common as summarized in You et al. (2019). This system is primarily controlled by the vertical distribution of temperature where temperature increases with depth.

Herein, we describe a unique horizontal sand layer where high-saturation free gas transitions to high-saturation hydrate in the Qiongdongnan Basin (QDNB) of the South China Sea (SCS). While a few horizontal gas to hydrate transitions have been noted before (Berndt et al., 2019; Bünz and Mienert, 2004), this QDNB system has documented, high saturations in a sand layer. Sand layers with high saturations of hydrate are of interest because they may be an energy resource and can also host a large amount of near-seafloor subsurface carbon (Archer, 2007; Boswell and Collett, 2011). How high-saturation hydrate forms within sand layers, however, is a topic of debate (You et al., 2019). Direct free gas flow into a sand layer is not thought to be a main mechanism of methane transport to sand reservoirs because hydrate will form once the gas moves into the hydrate stability zone, reducing permeability and impeding further gas flow into the sand layer.

This high-saturation horizontal sand in the QDNB was drilled during two recent drilling expeditions led by the Guangzhou Marine Geological Survey (GMGS) in May 2021 and September 2022. We document this system with 3D seismic, logging-while-drilling (LWD) data and in situ borehole temperature measurements. We show that this system is caused by the flow of hot fluids and gas through a vertical advective zone which leads to a large lateral temperature gradient in the shallow sand layer. In this system, free gas is stable near the advective zone and hydrate is stable in cooler surrounding region.

2 Geologic Setting

The QDNB is a Cenozoic rift basin located on the northwestern slope of the SCS. The evolution of the QDNB can be divided into two stages: an Eocene-Oligocene rift and a Neogene-Quaternary post-rift thermal subsidence (Hu et al., 2013; Ru & Pigott, 1986). The study area is near the Lingshui (LS18-1, etc.) and Yongle (Y8-1) conventional gas fields (Xie, 2014; Shi et al., 2019) and is located on the Songnan Low Uplift (SLU) of the QDNB (Fig. 1a, b). Above the uplift, there is a large seismic blanking zone associated with a gas chimney and a deep-rooted fault extends into the overlying shallow sedimentary system (Fig. 1c). Eight wells were drilled by GMGS in 2021 (GMGS8) and 2022 (GMGS9) exploring the high-amplitude reflections above the gas chimney.

3 Data and Methods

The seismic data was acquired in 2018 by GMGS and has a dominant frequency of 40 Hz and an inline and crossline spacing of 50 m and 6.25 m, respectively. The seismic data is shown in zero-phase with positive amplitudes represented by a red and yellow peak and negative amplitudes represented by a blue and cyan trough. During the drilling expeditions in 2021 and 2022, LWD data was measured by Schlumberger tools, including MicroScope HD, NeoScope, SonicScope and proVISION. In situ temperature measurements were collected in the borehole using a Fugro temperature cone penetrometer.

We use LWD data to identify lithologic changes and the presence of gas and hydrate (e.g. Goldberg et al., 2010). Minerals in sediment and fluid volumes are calculated by the Elemental Analysis (ELAN) method in commercial Techlog software (Text S1 and Fig. S1 in Supporting Information). The dip and azimuth of beds are picked from 360-degree borehole resistivity images (Bonner et al., 1996). Nuclear magnetic resonance (NMR) logging is used to measure the porosity of clay-rich intervals and the absolute permeability is calculated by Timur-Coates equation using NMR logging data (Yoneda et al., 2022).

4 Internal Structure

We interpret the internal structure of the flat-lying system using 3D seismic and LWD data from seven wells (Fig. 2). On the seismic data, Horizon A is a prominent, strong reflection that dips less than 1 degree and exhibits a phase reversal: high-amplitude positive reflections to the southwest and northeast switch to negative reflections at the middle of the seismic line just above the gas chimney (Fig. 2a). An amplitude attribute extraction from Horizon A shows that positive amplitudes concentrate in the southeast and negative amplitudes are associated with the deep-rooted fault and gas chimney (Fig. 2b). Seven wells were drilled into Horizon A to understand the distribution of gas and hydrate (Fig. 2).

Wells W08, W20 and W05 targeted the positive amplitude reflections on Horizon A (Fig. 2a, b). Horizon A at these well locations is characterized by low gamma ray values (~50 gAPI), high resistivity (~200 Ωm) and high P-wave velocity (＞3000 m/s), which indicates that highly concentrated hydrate occurs in coarse-grained sediments (Fig. 2c). The logs show Horizon A at the depth between 1892.6-1905.2 m below sea level (mbsl), 127-145.9 m below seafloor (mbsf) with a thickness of 3.9-9.2 m (Figure 2).

Wells W02, W03 and W19 were drilled on the Horizon A negative amplitude reflections (Fig. 2a). In W02 to W19, we observe changes in bulk density, neutron porosity, resistivity and P-wave velocity in Horizon A which allow us to interpret the presence of free gas and hydrate (Fig. 2c). Neutron porosity measures hydrogen concentration and when gas is present, the porosity value deceases relative to water saturated sediments because the lower concentration of hydrogen in free gas (Ellis & Singer, 2007); hydrate has little to no effect on neutron porosity. Bulk density notably decreases only when there is a large amount of gas in the pore space. Bulk density also decreases slightly when high saturations of hydrate are present (Goldberg et al., 2010). Because of these patterns, the crossover between the neutron porosity and bulk density logs is used as a gas indicator (highlighted with dashed boxes on Fig. 2c). P-wave velocity is also sensitive to free gas and drops significantly even when very small amounts of gas are present (e.g. Murphy et al., 1993).

The combination of low P-wave velocity (~1450 m/s), low neutron porosity (~ 0.17), a noticeable decrease bulk density (near 1.5 g/cm^3) and the large neutron-density crossover indicates that there is a large amount of free gas in W02. This agrees with the results from ELAN and the location of W02 on the strong, negative seismic amplitude (Fig. 2). In neighboring W03, the P-wave velocity is equally low in Horizon A, but the neutron porosity-density crossover is smaller and only in a thin interval of Horizon A from ~1891-1893 m. This indicates that at W03 Horizon A has a smaller amount of free gas than in W02. The high resistivity in W03 throughout Horizon A (~200 Ωm) indicates a high concentration of hydrate is also present. Therefore, W03 is located in a transition zone where free gas and hydrate co-exist in sands. W19, which is southeast of W03 and just on the edge of the positive amplitude map (Fig. 2) has high concentrations of hydrate, and possibly, a very small amount of free gas. There is a very slight crossover between the neutron and density indicating free gas may be present, but there is no significant decrease in P-wave velocity. Wells W08 and W20 were drilled outside of the negative amplitudes and have only high concentrations of hydrate in Horizon A, as shown by the high resistivity and high P-wave velocity.

W07 was drilled in the center of the gas chimney and drilling was halted due to a significant gas flow from the borehole. Two sand layers were encountered in this well. In the upper layer (1889.4-1892.4 mbsl, 122.1-125.1 mbsf) free-flowing gas was observed by ROV while drilling this section. The lower Horizon A (1895.9-1903.4 mbsl, 128.6-136.0 mbsf) is inferred as a gas-bearing sand layer without hydrate because of the dramatic increase in borehole size, the separation of the resistivity curves and a strong gas flow observed from the wellhead.

Overall, the well logs indicate that a high saturation free gas-bearing zone occurs in the center of the system and is enclosed by highly concentrated hydrate. A transition zone where free gas and hydrate co-exists occurs between the two endmembers.

5 Sedimentary Architecture

Using W05 as an example, we identify two types of important stratigraphic layers above Horizon A: mass-transport deposits (MTDs) and hemipelagic deposits (HDs) (Fig. 3a, b). MTDs are characterized by internal deformation (Shanmugam, 2021) and strong basal shear (Cardona et al., 2020). They can be identified in logging data by significant changes in the dip and/or azimuth of bedding within the MTD (Piper et al., 1997) and by densification at the base of the MTD (Dugan, 2012; Sawyer et al., 2009). Here, we identify three MTD units using the dip and azimuth of bedding changes and density increases (Fig. 3b). The amplitude attribute map indicates that the MTDs originate from the northern slope of the QDNB (Fig. 3c) and erode the underlying channelized turbidite lobe (Horizon A) with a clear erosional boundary in the northwest (Fig. 3d).

HDs are usually fine-grained, and generally have little deformation and consistent physical properties within the unit. However, at this site, the low bulk density and elevated MRP (NMR Porosity) occurred in the HDs (Fig. 3b), suggests shallow overpressure may have developed within them. The HDs are bounded by denser MTDs and highly concentrated hydrate-bearing sands, both of which may impede the movement of water and allow the buildup of pressure. The degree of overpressure is estimated by using the method from Long et al. (2011).

6 Mechanisms Controlling the Gas Hydrate Reservoir

6.1 Vertically focused fluid flow

The free gas in Horizon A is most likely the result of the underlying efficient focused fluid flow system that consists of the SLU, the deep-rooted fault and the shallow gas chimney (Fig. 1c). The SLU, as the most prominent rise structure in the region, is generally accepted to have ceased activity since 23 Ma (T60) following the thermal subsidence throughout the QDNB (Zhou et al., 2019), although the understanding of the evolution of the SLU is still limited.

The deep-rooted fault extending in a NE-SW direction developed along the steeper flank of the SLU and continues to grow upwards towards the seafloor. Because the QDNB was likely tectonically stable as the termination of SCS spreading at ~16 Ma (Wang & Li, 2009), we suggest differential compaction may account for this growing fault. There is about 2500~3000 m difference in depositional thickness between Lingshui Sag and the SLU (Fig. 1c), which could cause a large differential settlement during the long period of compaction. Tensile stress may concentrate within sediments just above the SLU and fracturing was likely promoted during this time. As a result, the fault along the steeper flank of the SLU was reactivated and grew upwards. Differential compaction is also suggested by the features of flexural bending on the seismic profile (Fig. 1c). Fluids from deeper in the sedimentary section converge towards the top of the SLU along the fault and SLU flanks, and then continue to flow upward towards Horizon A along the gas chimney feature, which we presume is composed of a large network of fractures.

6.2 Lateral fluid migration

When free gas and fluids migrating along the gas chimney reach Horizon A, the flow shifts in a lateral direction along the sand layer. This is supported by the very sharp increase of the resistivity in the hydrate-bearing sand layer from W05, which indicates gas flow may be completely sealed by the overlying sediments even though its absolute permeability is 1~10 mD (Fig. 3b). MTDs are often considered to be seals in traditional petroleum and hydrate systems (Cardona et al., 2020; Crutchley et al., 2021). However, in this location a HD not a MTD immediately overlies the sand layer (Fig. 3b), therefore, we suggest capillary sealing may be the mechanism responsible. Capillary sealing occurs at the interface between coarse (Horizon A) and fine-grained (HD3) sediments when two fluid phases (gas and water) are present (Cathles, 2001; Revil et al., 1998). In addition, overpressure occurred in HD3 may also enhance the seal capacity of overlying fine-grained sediments. Finally, hydrate itself could be self-sealing part of the Horizon A sand by blocking the pore space and preventing the migration of gas. In any case, sealing at or near the top of Horizon A results in lateral fluid migration along Horizon A.

6.3 Heat transfer

The in-situ borehole temperature was measured in W07 and W01 using a temperature cone penetrometer. W07 is located in the center of the advective zone where Horizon A has a high saturation of free gas (Figure 2) and W01 is several kilometers outside the free gas-hydrate system (Figure 1). The temperature measurements indicate a geothermal gradient of 103.7 °C/km in W07 and 65.8 °C/km in W01, with corresponding heat flows of 103.7 mW/m^2 and 65.8 mW/m^2 (assuming a thermal conductivity of 1 W/m·°C). The heat flow in the advective area is significantly elevated. Drilling results from W07 and W02 suggest very little or no hydrate is present in sands within the advective zone, which indicates the heat is the result of hot fluids and gas advection rather than the latent heat released during hydrate formation. This process of heat transfer to the subsurface from advecting hot fluids has been observed in the other settings such as Cascadia margin, Gulf of Mexico, Hakon Mosby Mud Volcano and offshore Costa Rica (Wood et al., 2002; Ruppel et al., 2005; Ginsburg et al., 1999; Kaul et al., 2006; Grevemeyer et al., 2004), however, none of these sites are a large, flat lying free gas-hydrate reservoir.

We use a two-dimensional heat transfer model to estimate the gas flux and temperature profile across W07 under a steady state that considers advecting methane from deep is consumed to form hydrate on the margins (Text S2 and Fig. S2, see detailed in the Supporting Information). The energy conservation equation is used to predict the temperature distribution in this site, which can be expressed as:

$$\frac{\partial^2 \lambda T}{\partial z^2} + \frac{\partial^2 \lambda T}{\partial x^2} + \frac{\partial c_g Q_{g,v} T}{\partial z} - \frac{\partial c_g Q_{g,l} T}{\partial x} = 0 \quad (1).$$

where z is the depth, x is the distance from the center of the advective zone, T is the geothermal temperature, λ = 1 W/m·°C is the bulk thermal conductivity (Liu & Flemings, 2006), c_g = 3500 J/kg is heat capacity of methane gas (Liu & Flemings, 2006), $Q_{g,v}$ is the upward gas flux in the advective zone, and $Q_{g,l}$ is the lateral gas flux along the sand layer. The total gas flux in the advective zone is $\pi R_c^2 \cdot Q_{g,v}$ (R_c =750 m, is the radius of the advective zone), and $Q_{g,l}$ can be expressed as:

$$Q_{g,l} = \frac{\pi R_c^2 \cdot Q_{g,v}}{\pi \cdot x \cdot H} = \frac{R_c^2 \cdot Q_{g,v}}{x \cdot H} \quad (2).$$

where H is the thickness of the sand layer.

In this model, we quantified this upward-doming temperature field and the base of the gas hydrate stability zone (BGHSZ) of this site (Fig. S2). $Q_{g,l}$ decreases with x resulting in a decrease in temperature with x. From W07 to the southern edge of the system (Fig. S2a, b), the temperature at the top of Horizon A (128 mbsf) decreases from 17.4 °C to 15.2 °C. We extract the temperature data at W07 from the model and it shows a good match with the in situ measured data (Fig. S2c). The BGHSZ is elevated by 106 m (from 234 m to 128 m) in the center of the advective zone. The estimated upward gas flux of 21 kg/m^2/yr is higher than average values from the documented seepage areas such as Hydrate Ridge, the Black Sea and the Norwegian continental margin (Heeschen et al., 2005; Sahling et al., 2009; Felden et al., 2010). This upward-doming temperature field controls the formation of the flat-lying transitional gas to hydrate system in the horizontal sand layer.

6.4 System formation

The formation of the flat-lying transitional system at this site can be summarized in four steps (Fig. 4). First, the Horizon A sand was deposited on the SLU and was subsequently covered by HDs and MTDs. Second, hot fluids and methane gas were funneled into the fault and gas chimney and advected toward Horizon A; differential compaction may also have played a role in this focused fluid flow. Third, sealing occurred at the interface of Horizon A and HD3, which prevented fluids from continuing their upward trajectory and redirected the fluids to migrate laterally along Horizon A. Lastly, the heat that accompanied the advecting fluids resulted in an upward-doming temperature field that has significantly higher geothermal temperatures in the advective zone and lower temperatures at its margin. As a result, hydrate is not stable in Horizon A within the advective zone, while hydrate is stable on the margins outside of the advective zone.

6.5 Geological implications

You et al. (2019) emphasized that methane transport controls the formation of different types of hydrate. In sand reservoirs with high saturations of hydrate, however, heat flow and heat carried by migrating fluids has not been considered a primary mechanism of methane transport to sand reservoirs in the hydrate stability zone. Instead, the prevailing methane migration models for hydrate bearing sand reservoirs reviewed by You et al. (2019) include local methane diffusion (Malinverno, 2010), diffusion with overpressure (Nole et al., 2016), salt exclusion and salinity variations allowing free gas flow (You and Flemings 2018), and the solidification of gas reservoirs resulting from changing climatic conditions over time (Behseresht and Bryant, 2012). Herein, we show that focused heat supplied through deep advecting hot fluids creates a lateral geothermal gradient in a horizontal sand reservoir that causes a lateral transition from free gas to hydrate. This site shows that heat flow is an important factor that controls the distribution of the hydrate system in sand reservoirs and should be considered in hydrate system formation and characterization.

Advecting hot fluids are certainly a key factor causing the formation of the flat-lying gas to hydrate transitional system, however, the occurrence of the coarse-grained sand layer is also very important for the development of this system. Our heat transfer model indicates high gas flux present here but the horizontal sand layer with low capillary entry pressure (You et al., 2021) would reduce the gas column height and pressure by lateral porous flow. Otherwise, vertical gas-driven tensile fracturing would occur at this shallow depth and most of gas would seep out of the seafloor (Daigle et al., 2020). Therefore, a large amount of methane gas is sequestered in this system as free gas and hydrate rather than vent into the ocean as commonly found in mud-rich settings.

High-amplitude seismic reflections with the polarity of the seafloor above the BSR are generally noted as the most promising indicator for the presence of concentrated hydrate and have been widely used in global hydrate exploration (Boswell et al., 2012; Boswell et al., 2016; Noguchi et al., 2011; Yoo et al., 2013; Shukla et al., 2019). However, this study suggests that high-amplitude reflections coincident with the BSR could also indicate the presence of hydrate, especially in sand reservoirs, and cannot be neglected in exploration.

7 Conclusions

We describe a flat-lying, free gas to gas hydrate transitional system in a sand reservoir. Unlike gas hydrate accumulating in dipping sands in the Gulf of Mexico and Nankai Trough where fluids can migrate upward by buoyancy along the permeable sand layer toward the BGHSZ, a flat-lying sand reservoir changes the path of fluid migration and also the distribution of the free gas and hydrate. The deep-sourced fluid flow not only provides sufficient gas but also advects a significant amount of heat to the shallow subsurface, which results in an upward perturbation on the BGHSZ and free gas into the regional GHSZ (defined by the background geothermal gradient of 65.8 °C/km in W01). Capillary sealing leads to a lateral migration of the hot fluids and gas along the flat-lying sand layer. Hydrate forms when the temperature decreases as the free gas moves away from the advective zone. This site shows that temperature can have significant control on hydrate formation in sands and may be a key mechanism which allows gas migration within the GHSZ and hydrate formation in high-saturation hydrate filled sands.

Acknowledgments

The crew and scientists of GMGS8 and GMGS9 gas drilling expedition is appreciated for their outstanding work. We gratefully acknowledge Timothy Collett and anonymous reviewers for their valuable comments. This study was funded by the National Natural Science Foundation of China (Grant No. 42276083), Guangdong Major Project of Basic and Applied Basic Research (No.2020B0301030003) and National Key Research and Development Program of China (2021YFC2800901). A. Cook was supported by the US NSF # 1752882.

Data Availability Statement

Data is available at Kuang et al. (2023).

References

Archer, D. (2007), Methane hydrate stability and anthropogenic climate change, Biogeosciences, 4(4), 521-544. https://doi.org/10.5194/bg-4-521-2007.

Behseresht, J., and S. L. Bryant (2012), Sedimentological control on saturation distribution in Arctic gas-hydrate-bearing sands, Earth and Planetary Science Letters, 341–344(0), 114-127. https://doi.org/10.1016/j.epsl.2012.06.019.

Berndt, C., Chi, W.C., Jegen, M., Lebas, E., Crutchley, G., Muff, S., Hölz, S., Sommer, M., Lin, S., Liu, C.S. and Lin, A.T., 2019. Tectonic controls on gas hydrate distribution off SW Taiwan. Journal of Geophysical Research: Solid Earth, 124(2), pp.1164-1184.

Bonner, S., Fredette, M., Lovell, J., Montaron, B., Rosthal, R., Tabanou, J., Wu, P., Clark, B., Mills, R., and Williams, R (1996), Resistivity while drilling—images from the string, Oilfield Rev, 8(1):4–19.

Boswell, R., and T. S. Collett (2011), Current perspectives on gas hydrate resources, Energy & Environmental Science, 4(4), 1206-1215. https://doi.org/10.1039/C0EE00203H

Boswell, R., T. S. Collett, M. Frye, W. Shedd, D. R. McConnell, and D. Shelander (2012), Subsurface gas hydrates in the northern Gulf of Mexico, Marine and Petroleum Geology, 34(1), 4-30. https://doi.org/10.1016/j.marpetgeo.2011.10.003.

Boswell, R., C. Shipp, T. Reichel, D. Shelander, T. Saeki, M. Frye, W. Shedd, T. S. Collett, and D. R. McConnell (2016), Prospecting for marine gas hydrate resources, Interpretation, 4(1), SA13-SA24. https://doi.org/10.1190/int-2015-0036.1.

Bünz, S. and Mienert, J., 2004. Acoustic imaging of gas hydrate and free gas at the

Storegga Slide. Journal of Geophysical Research: Solid Earth, 109(B4).

Cardona, S., L. J. Wood, B. Dugan, Z. Jobe, and L. J. Strachan (2020), Characterization of the Rapanui mass-transport deposit and the basal shear zone: Mount Messenger Formation, Taranaki Basin, New Zealand, Sedimentology, 67(4), 2111-2148. https://doi.org/10.1111/sed.12697.

Cathles, L. (2001), Capillary Seals as a Cause of Pressure Compartmentation in Sedimentary Basins, Petroleum Systems of Deep-Water Basins: Global and Gulf of Mexico Experience, Houston, Texas, GCSSEPM, GCS 021. https://doi.org/10.5724/gcs.01.21.0561

Cheng, C., T. Jiang, Z. Kuang, J. Ren, J. Liang, H. Lai, and P. Xiong (2021), Seismic characteristics and distributions of Quaternary mass transport deposits in the Qiongdongnan Basin, northern South China Sea, Marine and Petroleum Geology, 129, 105118. https://doi.org/10.1016/j.marpetgeo.2021.105118.

Crutchley, G. J., J. J. Mountjoy, J. I. T. Hillman, F. Turco, S. Watson, P. B. Flemings, B. Davy, S. Woelz, A. R. Gorman, and J. Bialas (2021), Upward-Doming Zones of Gas Hydrate and Free Gas at the Bases of Gas Chimneys, New Zealand's Hikurangi Margin, Journal of Geophysical Research: Solid Earth, 126(9), e2020JB021489. https://doi.org/10.1029/2020JB021489.

Daigle, H., A. Cook, Y. Fang, A. Bihani, W. Song, and P. B. Flemings (2020), Gas-Driven Tensile Fracturing in Shallow Marine Sediments, Journal of Geophysical Research: Solid Earth, 125(12), e2020JB020835. https://doi.org/10.1029/2020JB020835.

Dugan, B. (2012), Petrophysical and consolidation behavior of mass transport deposits from the northern Gulf of Mexico, IODP Expedition 308, Marine Geology, 315-318, 98-107. https://doi.org/10.1016/j.margeo.2012.05.001.

Ellis, D. V., and J. M. Singer (2007), Introduction to Well Log Interpretation: Finding the Hydrocarbon, in Well Logging for Earth Scientists, edited by D. V. Ellis and J. M. Singer, pp. 17-39, Springer Netherlands, Dordrecht. https://doi.org/10.1007/978-1-4020-4602-5_2.

Felden, J., F. Wenzhöfer, T. Feseker, and A. Boetius (2010), Transport and consumption of oxygen and methane in different habitats of the Håkon Mosby Mud Volcano (HMMV), Limnology and Oceanography, 55(6), 2366-2380. https://doi.org/10.4319/lo.2010.55.6.2366.

Ginsburg, G. D., A. V. Milkov, V. A. Soloviev, A. V. Egorov, G. A. Cherkashev, P. R. Vogt, K. Crane, T. D. Lorenson, and M. D. Khutorskoy (1999), Gas hydrate accumulation at the Håkon Mosby Mud Volcano, Geo-Marine Letters, 19(1), 57-67. https://doi.org/10.1007/s003670050093.

Goldberg, D. S., R. L. Kleinberg, J. L. Weinberger, A. Malinverno, P. J. McLellan, and T. S. Collett (2010), 16. Evaluation of Natural Gas-Hydrate Systems Using Borehole Logs, in Geophysical Characterization of Gas Hydrates, edited by M. Riedel, E. C. Willoughby and S. Chopra, pp. 239-261, Society of Exploration Geophysicists. https://doi.org/10.1190/1.9781560802197.ch16.

Grevemeyer, I., et al. (2004), Fluid flow through active mud dome Mound Culebra offshore Nicoya Peninsula, Costa Rica: evidence from heat flow surveying, Marine Geology, 207(1), 145-157. https://doi.org/10.1016/j.margeo.2004.04.002.

Haacke, R. R., G. K. Westbrook, and R. D. Hyndman (2007), Gas hydrate, fluid flow and free gas: Formation of the bottom-simulating reflector, Earth and Planetary Science Letters, 261(3), 407-420. https://doi.org/10.1016/j.epsl.2007.07.008.

Heeschen, K. U., R. W. Collier, M. A. de Angelis, E. Suess, G. Rehder, P. Linke, and G. P. Klinkhammer (2005), Methane sources, distributions, and fluxes from cold vent sites at Hydrate Ridge, Cascadia Margin, Global Biogeochemical Cycles, 19(2), GB2016. https://doi.org/10.1029/2004gb002266.

Hu, B., L. Wang, W. Yan, S. Liu, D. Cai, G. Zhang, K. Zhong, J. Pei, and B. Sun (2013), The tectonic evolution of the Qiongdongnan Basin in the northern margin of the South China Sea, Journal of Asian Earth Sciences, 77, 163-182. https://doi.org/10.1016/j.jseaes.2013.08.022.

Kaul, N., J. P. Foucher, and M. Heesemann (2006), Estimating mud expulsion rates from temperature measurements on Håkon Mosby Mud Volcano, SW Barents Sea, Marine Geology, 229(1), 1-14. https://doi.org/10.1016/j.margeo.2006.02.004.

Kuang Z., A. Cook, J. Ren, W. Deng, Y. Cao, and H. Cai. (2023). A Flat-lying Transitional Free Gas to Gas Hydrate System in a Sand Layer in the Qiongdongnan Basin of the South China Sea [Dataset]. Zenodo. https://doi.org/10.5281/zenodo.7721790.

Kvenvolden, K. A., and T. D. Lorenson (2001), The Global Occurrence of Natural Gas

Hydrates, in Natural Gas Hydrates: Occurrence, Distribution, and Detection, edited by C. K. Paull and W. P. Dillon, pp. 3-18, American Geophysical Union, Washington, DC. https://doi.org/10.1029/GM124p0003.

Liu, X., and P. B. Flemings (2006), Passing gas through the hydrate stability zone at southern Hydrate Ridge, offshore Oregon, Earth and Planetary Science Letters, 241(1–2), 211-226. http://dx.doi.org/10.1016/j.epsl.2005.10.026.

Long, H., P. B. Flemings, J. T. Germaine, and D. M. Saffer (2011), Consolidation and overpressure near the seafloor in the Ursa Basin, Deepwater Gulf of Mexico, Earth and Planetary Science Letters, 305(1), 11-20. https://doi.org/10.1016/j.epsl.2011.02.007.

Malinverno, A. (2010), Marine gas hydrates in thin sand layers that soak up microbial methane, Earth and Planetary Science Letters, 292(2010), 399-408. https://doi.org/10.1016/j.epsl.2010.02.008.

Murphy, W., A. Reischer, and K. Hsu (1993), Modulus decomposition of compressional and shear velocities in sand bodies, GEOPHYSICS, 58(2), 227-239. https://doi.org/10.1190/1.1443408.

Noguchi, S., N. Shimoda, O. Takano, N. Oikawa, T. Inamori, T. Saeki, and T. Fujii (2011), 3-D internal architecture of methane hydrate-bearing turbidite channels in the eastern Nankai Trough, Japan, marine and Petroleum Geology(2011), 1-12. https://doi.org/10.1016/j.marpetgeo.2011.02.004.

Nole, M., H. Daigle, A. E. Cook, and A. Malinverno (2016), Short-range, overpressure-driven methane migration in coarse-grained gas hydrate reservoirs, Geophysical

Research Letters, 43(18), 9500-9508. https://doi.org/10.1002/2016GL070096.

Piper, D. J. W., C. Pirmez, P. L. Manley, D. Long, R. D. Flood, W. R. Normark, and W. Showers (1997), Mass-transport deposits of the Amazon fan, in Proceedings of the Ocean Drilling Program, Scientific Results, edited by R. D. Flood, D. J. W. Piper, A. Klaus and L. C. Peterson, pp. 109-146. https://doi.org/10.2973/odp.proc.sr.155.212.1997.

Revil, A., L. M. Cathles III, J. D. Shosa, P. A. Pezard, and F. D. de Larouzière (1998), Capillary sealing in sedimentary basins: A clear field example, Geophysical Research Letters, 25(3), 389-392. https://doi.org/10.1029/97GL03775.

Ru, K., and J. D. Pigott (1986), Episodic Rifting and Subsidence in the South China Sea1, AAPG Bulletin, 70(9), 1136-1155. https://doi.org/10.1306/94886a8d-1704-11d7-8645000102c1865d.

Ruppel, C., G. R. Dickens, D. G. Castellini, W. Gilhooly, and D. Lizarralde (2005), Heat and salt inhibition of gas hydrate formation in the northern Gulf of Mexico, Geophysical Research Letters, 32(4), L04605. https://doi.org/10.1029/2004GL021909.

Sahling, H., et al. (2009), Vodyanitskii mud volcano, Sorokin trough, Black Sea: Geological characterization and quantification of gas bubble streams, Marine and Petroleum Geology, 26(9), 1799-1811. http://dx.doi.org/10.1016/j.marpetgeo.2009.01.010.

Sawyer, D. E., P. B. Flemings, B. Dugan, and J. T. Germaine (2009), Retrogressive failures recorded in mass transport deposits in the Ursa Basin, Northern Gulf of

Mexico, Journal of Geophysical Research: Solid Earth, 114(B10). https://doi.org/10.1029/2008JB006159.

Shanmugam, G. (2021), Chapter 2 - Mass transport: slides, slumps, and debris flows, in Mass Transport, Gravity Flows, and Bottom Currents, edited by G. Shanmugam, pp. 7-88, Elsevier. https://doi.org/10.1016/B978-0-12-822576-9.00002-3.

Shedd, W., R. Boswell, M. Frye, P. Godfriaux, and K. Kramer (2012), Occurrence and nature of "bottom simulating reflectors" in the northern Gulf of Mexico, Marine and Petroleum Geology, 34(1), 31-40. https://doi.org/10.1016/j.marpetgeo.2011.08.005.

Shi, H., J. Yang, Y. Zhang, J. Gan, and J. Yang (2019), Geological understanding innovation and major breakthrough to natural gas exploration in deep water in Qiongdongnan Basin, China Petroleum Exploration, 24(6), 691-698. https://doi.org/10.3969/j.issn.1672-7703.2019.06.001 (in Chinese with English abstract).

Shukla, K. M., T. S. Collett, P. Kumar, U. S. Yadav, R. Boswell, M. Frye, M. Riedel, I. Kaur, and K. Vishwanath (2019), National Gas Hydrate Program expedition 02: Identification of gas hydrate prospects in the Krishna-Godavari Basin, offshore India, Marine and Petroleum Geology, 108, 167-184. https://doi.org/10.1016/j.marpetgeo.2018.11.013.

Sloan, E. D., and C. Koh (2007), Clathrate hydrates of natural gases, CRC Press, Boca Raton.

Wang, P., and Q. Li (2009), History of the South China Sea – A Synthesis, in The South China Sea-Paleoceanography and Sedimentology, edited by P. Wang and Q. Li, pp. 485-496, springer.

Wood, W. T., J. F. Gettrust, N. R. Chapman, G. D. Spence, and R. D. Hyndman (2002), Decreased stability of methane hydrates in marine sediments owing to phase-boundary roughness, Nature, 420(6916), 656-660. https://doi.org/10.1038/nature01263.

Xie, Y. (2014), Significant breakthrough in proprietary deepwater natural gas exploration in the northern South China Sea and its inspiration, Natural Gas Industry B, 1(2), 221-229. https://doi.org/10.1016/j.ngib.2014.11.015.

Yoneda, J., Y. Jin, M. Muraoka, M. Oshima, K. Suzuki, W. F. Waite, and P. B. Flemings (2022), Comprehensive pressure core analysis for hydrate-bearing sediments from Gulf of Mexico Green Canyon Block 955, including assessments of geomechanical viscous behavior and nuclear magnetic resonance permeability, AAPG Bulletin, 106(5), 1143-1177. https://doi.org/10.1306/04272120204.

Yoo, D. G., N. K. Kang, B. Y. Yi, G. Y. Kim, B. J. Ryu, K. Lee, G. H. Lee, and M. Riedel (2013), Occurrence and seismic characteristics of gas hydrate in the Ulleung Basin, East Sea, Marine and Petroleum Geology, 47, 236-247. http://dx.doi.org/10.1016/j.marpetgeo.2013.07.001.

You, K., and P. B. Flemings (2018), Methane Hydrate Formation in Thick Sandstones by Free Gas Flow, Journal of Geophysical Research: Solid Earth, 123(6), 4582-4600. https://doi.org/10.1029/2018JB015683

You, K., P. B. Flemings, A. Malinverno, T. S. Collett, and K. Darnell (2019), Mechanisms of Methane Hydrate Formation in Geological Systems, Reviews of Geophysics, 57(4), 1146-1196. https://doi.org/10.1029/2018RG000638.

You, K., L. Summa, P. Flemings, M. Santra, and Y. Fang (2021), Three-Dimensional Free Gas Flow Focuses Basin-Wide Microbial Methane to Concentrated Methane Hydrate Reservoirs in Geological System, Journal of Geophysical Research: Solid Earth, 126(12), e2021JB022793. https://doi.org/10.1029/2021JB022793.

Zhou, J., X. Yang, J. Yang, J. Gan, H. Wu, X. He, and B. Hu (2019), Structure-Sedimentary Evolution and Gas Accumulation of Paleogene in Songnan Low Uplift of the Qiongdongnan Basin, Earth Science, 44(8), 2704-2716. https://doi.org/10.3799/dqkx.2019.104 (in Chinese with English abstract).

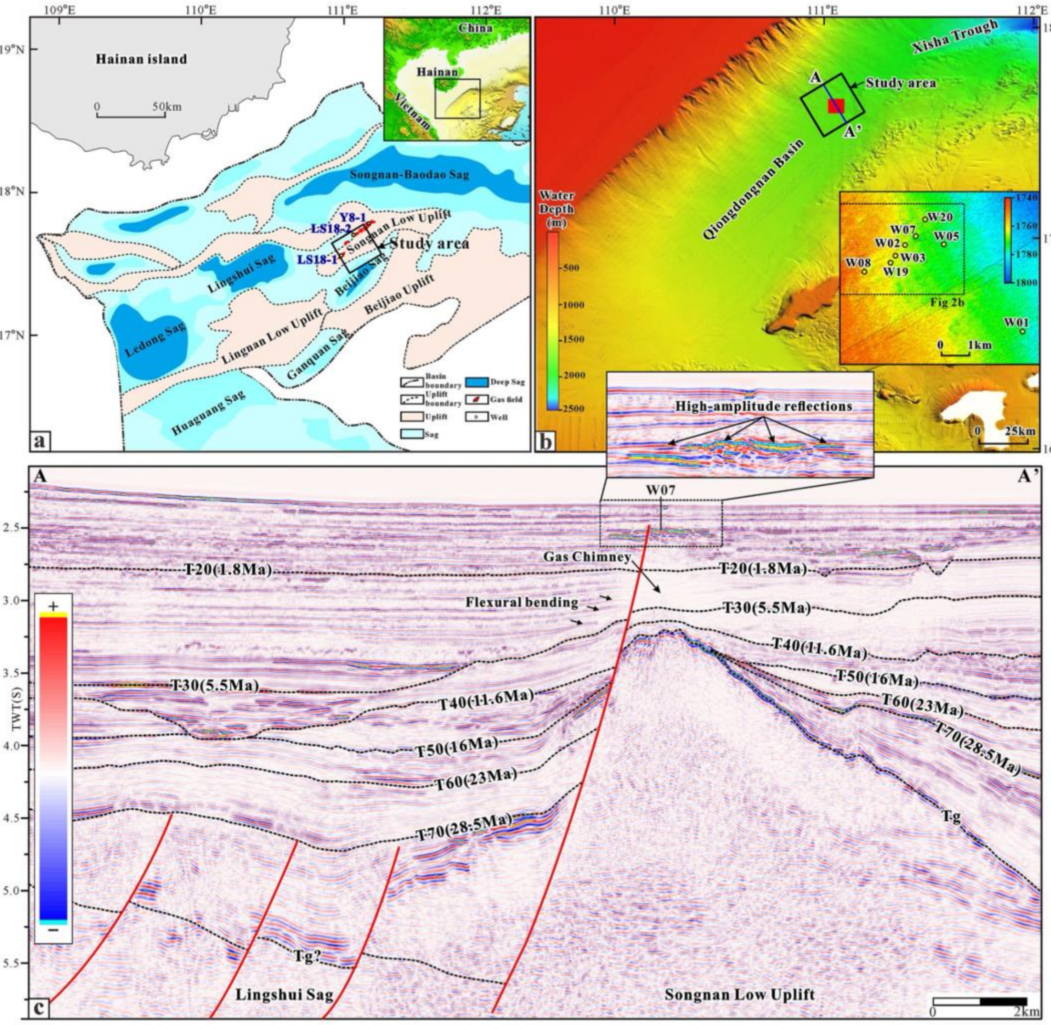

Fig 1. a: Location and structural units of the study area in the Qiongdongnan Basin (QDNB). The inset box indicates the location of Fig. 1a. b: Multibeam bathymetry map of the QDNB and locations of the study area, seismic profile and wells. The red filled box is the location of the inset. c: 3D seismic profile a-a' showing the major structural units including Lingshui Sag and Songnan Low Uplift, the stratigraphic framework (modified from Cheng et al., 2021), the gas chimney and high-amplitude reflections associated with Horizon A. Note the flexural bending occurred between T20 to T30, which may indicate the effect of differential compaction.

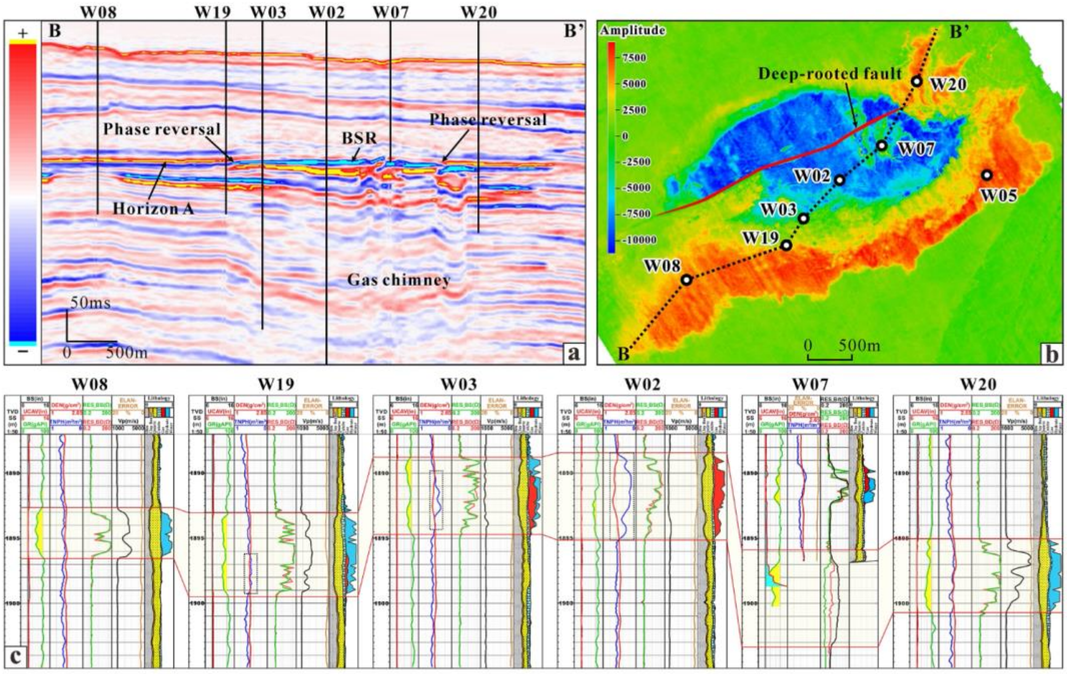

Fig 2. a: Cross-wells section showing the seismic reflection characteristics of Horizon A and the underlying gas chimney. b: Amplitude attribute map of Horizon A indicating the distribution of free gas (blue) and hydrate (red). The location is indicated in Fig. 1b. Note the distribution of the deep-rooted fault (filled with red). c: Multi-well correlation showing the log response of gas- and hydrate-bearing sands. The neutron-density crossover marked by black dashed boxes and the associated low Vp indicates the presence of free gas. Note the error of ELAN method is ~2%. TVDSS: true vertical depth subsea; BS: bit size; UCAV: ultrasonic caliper average; GR: gamma ray; DEN: bulk density; TNPH: thermal neutron porosity; RES_BS: shallow button resistivity; RES_BD: deep button resistivity; RES_Bit: bit resistivity; ELAN-ERROR: the error of ELAN method; Vp: P-wave velocity; Lithology: mineral and fluid volume fraction in sediment.

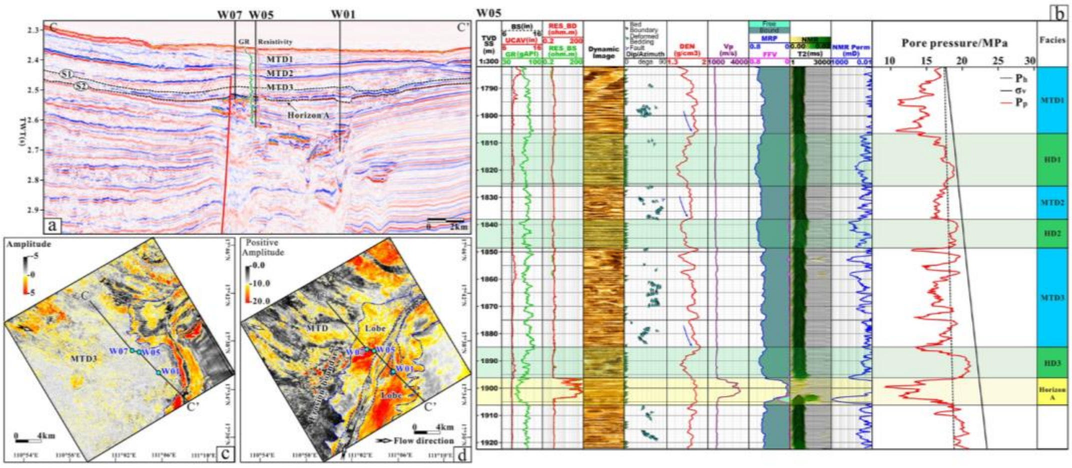

Fig 3. a: Cross-wells section showing the seismic reflection characteristics of Horizon A and MTDs. b: Detailed analysis of the log response of MTDs, HDs and hydrate-bearing sands. Dynamic image: dynamic resistivity image; Dip/Azimuth: the dip and azimuth of the sedimentary bedding; MRP: nuclear magnetic resonance (NMR) porosity; FFV: free fluid volume; T2: NMR T2 relaxation distributions; NMR perm: absolute permeability from Timur-Coates method; Shallow overpressure occurred in HDs is estimated. P_h, σ_v and P_p is the hydrostatic, lithostatic and pore pressure, respectively. Facies: sedimentary facies; MTD: mass transport deposit; HD: hemiplegic deposit; c-d: Amplitude attribute along horizon S1(c) and S2 (d) in Fig. 3a showing the distribution of the MTD and turbidite lobe.

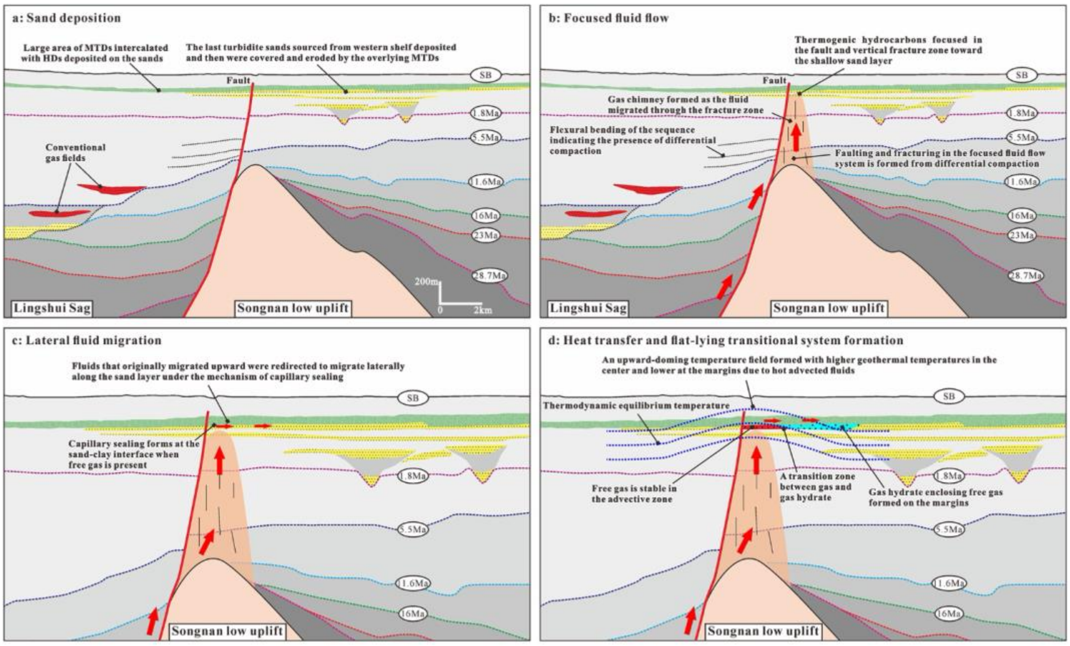

Fig 4. The geological processes and mechanisms forming the flat-lying gas to hydrate system in the sand.